Assessing the Quality of SeaWinds Rain Measurements

David W. Draper and David G. Long, *Senior Member, IEEE*

***Abstract*—While SeaWinds was designed to measure ocean winds, it can also measure rain over the ocean. SeaWinds on QuikSCAT active measurements of integrated columnar rain rate obtained via simultaneous wind/rain retrieval are evaluated via Monte Carlo simulation and the Cramér–Rao lower bound on estimate accuracy. Although sufficiently accurate in many conditions, the simultaneous wind/rain retrieval method used with SeaWinds on QuikSCAT data is ill-conditioned for certain wind directions and measurement geometries, sometimes yielding spurious rain rates in zero-rain conditions. To assess the validity of SeaWinds-derived rain rates, a simple empirically based rain thresholding scheme is presented, derived from simulated data. Thresholded QuikSCAT rain rates are compared to Tropical Rainfall Measuring Mission Microwave Imager monthly-averaged data, demonstrating good correlation for monthly-averaged data.**

***Index Terms*—Maximum likelihood, SeaWinds, scatterometer, simultaneous wind/rain retrieval, Tropical Rainfall Measuring Mission (TRMM) Microwave Imager (TMI).**

I. Introduction

RADAR backscatter at midrange incidence angles is driven mainly by Bragg scattering from small gravity-capillary waves induced by wind stress [1]. For Ku-band instruments such as SeaWinds, the backscatter is also sensitive to scattering and attenuation from falling rain droplets, as well as the small ripples created by rain striking the surface [2]–[6]. Although the accuracy of retrieved winds is degraded during rain events, the rain sensitivity of the Ku-band signal affords scatterometer-based retrieval of the vertically integrated rain rate [7]. This serendipitous application of SeaWinds data can be used to help fill gaps in coverage from other passive and active rain sensors.

In order to measure rain from SeaWinds and mitigate the effects of rain on the scatterometer wind data, Draper and Long [7] developed a simultaneous wind/rain retrieval method for use with SeaWinds on QuikSCAT data. The simultaneous wind/rain retrieval method uses a maximum-likelihood estimator to retrieve the wind speed, wind direction, and integrated rain rate from the SeaWinds backscatter measurements. Considering that SeaWinds was not intended to measure rain, simulations and validation given here and in [7] indicate that simultaneous wind/rain retrieval is surprisingly accurate, especially in the sweet spots of SeaWinds swath and when the true wind direction is not oriented in the cross-swath direction.

Manuscript received December 24, 2003; revised March 3, 2004.

D. W. Draper was with the Microwave Earth Remote Sensing Laboratory, Brigham Young University, Provo, UT 84602 USA. He is now with Ball Aerospace, Boulder, CO 80301 USA.

D. G. Long is with the Microwave Earth Remote Sensing Laboratory, Brigham Young University, Provo, UT 84602 USA (e-mail: long@byu.edu).

Digital Object Identifier 10.1109/TGRS.2004.828194

Although the method works well in many conditions, retrieving rain from the SeaWinds scatterometer has limitations. The main insufficiency in the method is related to the fact that wind and rain do not have orthogonal effects on ocean backscatter. Depending on the wind direction and measurement geometry, backscatter due to wind can be confused with the response from rain. This issue is a main source of frustration in creating accurate standalone rain flags from SeaWinds data. The effects of this identifiability problem is most noticeable when the wind is oriented cross swath, often yielding spurious rain rate solutions in zero-rain conditions. With wind in a cross-swath orientation, the backscatter response is similar between the fore and aft beams, appearing isotropic, a signature similar to rain. However, when the wind is not oriented cross swath, the wind and rain backscatter signatures are often quite different, affording better separation of wind and rain effects.

This paper addresses two main questions involved with SeaWinds rain estimation: "How accurate are the rain data?" and "For what conditions are the data valid?" To address the first question, rain rate measurement accuracy is assessed via Monte Carlo simulations and the Cramér–Rao (C–R) theoretical lower bound on retrieval accuracy. The C–R bound affords a computationally efficient method of theoretically estimating the covariance of the scatterometer-derived wind and rain rates. We address the second question by introducing a rain rate thresholding scheme that identifies the minimum believable rain rate estimate given the wind conditions. The threshold is set higher where spurious rain rates are more likely to occur, producing constant false-alarm performance at the risk of missed rain detections. The thresholds are validated against Precipitation Radar (PR) data from the Tropical Rainfall Measuring Mission (TRMM) and the SeaWinds multidimensional histogram (MUDH) rain flag. The comparison suggests that using the thresholds with simultaneous wind/rain retrieval can improve the existing SeaWinds rain detection accuracy for low rain rates (less than 5 km $\cdot$ mm/h).

We expand the validation given in [7], by comparing monthly-average rainfall statistics between QuikSCAT data and the TRMM Microwave Imager (TMI) [8]. Monthly-averaged QuikSCAT rain rates (although noisy) are well matched to TMI-derived monthly-average rain rates, with a correlation coefficient of about 0.7 and a small negative bias.

After presenting background to the SeaWinds instrument and simultaneous wind/rain retrieval in Section II, we analyze the quality of SeaWinds active rain measurements via the Cramér–Rao bound and simulation statistics in Section III. In Section IV, the simultaneous wind/rain retrieval-based rain rate thresholding scheme is presented, and validation of QuikSCAT monthly rainfall estimates with TMI data are given in Section V.

II. Background

The SeaWinds instrument employs a rotating pencil beam antenna with two offset feeds to measure the normalized backscattering cross section σ° of the ocean surface at surface incidences of 46° (H-polarization) and 54° (V-polarization). The antennas trace helical patterns on the surface with the inner H-polarization beam coverage extending approximately 700 km from nadir, and the outer V-polarization beam extending approximately 900 km from nadir. In order to retrieve winds, the inner beam region is observed from four different azimuth angles: two for each beam, fore and aft. The outer-beam-only region (swath edge) is only observed from the V-polarization beam [9].

Standard SeaWinds processing segments the σ° measurements on a 25-km wind vector cell (WVC) grid. The multiple measurements at each WVC are used to form a wind vector estimate. Wind is estimated by inverting the empirical relationship between the vector wind and σ° known as the geophysical model function (GMF), typically via maximum-likelihood estimation (MLE). Because of the symmetric nature of the GMF and measurement noise, the MLE generally produces several possible wind vector solutions known as ambiguities. The ambiguities are ranked according to likelihood, and the first ambiguity is not always the closest to the true wind. Thus, a second ambiguity selection step is typically employed in which a unique ambiguity field is chosen based on outside data (nudging), and modified median filtering [10], [11].

The outer nine WVCs on each side of the swath correspond to the outer-beam-only region. In this region, instrument skill (probability of a correct first ambiguity) is rather low. Also, in the center ~18 WVCs (nadir region), the viewing geometry for multiple measurements is somewhat poor, as the difference in azimuth angles for the two beams approaches 180°. The nadir region generally produces much noisier winds than the rest of the swath. However, the viewing geometry for the two off-nadir inner-beam regions, known as the "sweet spots," is very good for accurate wind retrieval [9], [12].

During rain, the backscatter response of the ocean is attenuated by falling hydrometeors. In addition, the nominal backscatter response is augmented by both scattering from falling rain, and surface ripples formed by rain striking the water. These effects can be modeled as a net attenuation from the nominal surface backscatter, and a net effective backscatter response

$$\sigma_m = \sigma_w \alpha_r + \sigma_e \tag{1}$$

where σ_m is the observed backscatter, σ_w is the contribution to backscatter from the wind-roughened seas, α_r is the two-way path-integrated attenuation factor from rain, and σ_e is the effective backscatter augmentation due to both surface and atmospheric rain effects. A parametric model for the attenuation α_r and effective rain backscatter σ_e as a function of integrated rain rate R is computed in [6]. The parametric model has the form

$$\alpha_r(R) = 10^{-10^{f_a(R_{\rm dB})/10}/10} \tag{2}$$

$$\sigma_e(R) = 10^{f_e(R_{\rm dB})/10} \tag{3}$$

where $R_{\rm dB} = 10\log_{10} R$, and $f_a(R_{\rm dB})$ and $f_e(R_{\rm dB})$ are defined as second-order polynomials in $R_{\rm dB}$

$$f_a(R_{\rm dB}) = \sum_{n=0}^{2} x_a(n) R_{\rm dB}^n \tag{4}$$

$$f_e(R_{\rm dB}) = \sum_{n=0}^{2} x_e(n) R_{\rm dB}^n. \tag{5}$$

The coefficients $x_a(n)$ and $x_e(n), n = 0\ldots2$ are computed in [6] via comparison with three months of colocated TRMM PR/QuikSCAT data.

Using this simple model for the backscatter due to rain, simultaneous wind/rain retrieval is possible from SeaWinds data [7]. The simultaneous wind/rain retrieval uses an MLE technique, much like the standard wind-only method. The measurement model assumes Gaussian statistics for the noise, yielding a measurement probability density of the form

$$p(\mathbf{z} \,|\, u, d, R) = \prod_k \frac{1}{\sqrt{2\pi}\varsigma_{rk}} \exp\left\{-\frac{1}{2}\frac{(z_k - \mathcal{M}_{rk})^2}{\varsigma_{rk}^2}\right\} \tag{6}$$

where k indexes the backscatter measurements $\mathbf{z}$ in the WVC, u is the wind speed, and d is the wind direction. In (6), the mean and variance are equal to

$$\mathcal{M}_{rk} = \mathcal{M}_k \alpha_{rk} + \sigma_{ek} \tag{7}$$

$$\varsigma_{rk} = (1+\alpha_k)\epsilon_k + \alpha_k \mathcal{M}_{rk}^2 + \beta_k \mathcal{M}_{rk} + \gamma_k \tag{8}$$

where α_k, β_k, and γ_k are the communication noise coefficients of the kth measurement [13], and the following simplified notation is used where the dependence on wind and rain is implied:

$$\mathcal{M}_k = \mathcal{M}(u, d - \phi_k, \theta_k, \mathrm{pol}_k) \tag{9}$$

$$\alpha_{rk} = \alpha_r(R, \mathrm{pol}_k) \tag{10}$$

$$\sigma_{ek} = \sigma_e(R, \mathrm{pol}_k) \tag{11}$$

where $\mathcal{M}$ is the GMF, ϕ_k is the antenna azimuth angle, θ_k is the incidence angle, pol_k is the polarization of the kth measurement, and ϵ_k is defined as

$$\epsilon_k = (K_{pm}\alpha_{rk}\mathcal{M}_k + K_{pe}\sigma_{ek})^2 \tag{12}$$

where K_{pm} and K_{pe} represent the normalized standard deviation of the GMF and effective rain backscatter, respectively [7], [12].

The general MLE method involves finding the wind/rain combination that maximizes the probability distribution given in (6) given the measured σ° values [14]. The probability distribution can be rewritten as a log-likelihood function of the form

$$L(u, d, R) = -\frac{1}{2}\sum_k \left\{\log(2\pi) + \log\varsigma_k^2 + \frac{(z_k - \mathcal{M}_{rk})^2}{\varsigma_k^2}\right\}. \tag{13}$$

For use with SeaWinds, the log-likelihood function is further simplified by dropping the first two terms inside the brackets, and multiplying by -2, yielding

$$l(u, d, R) = \sum_k \frac{(z_k - \mathcal{M}_{rk})^2}{\varsigma_k^2}. \tag{14}$$

The wind and rain are simultaneously estimated by minimizing the simplified likelihood function.

As with the standard wind-only procedure, the likelihood function has several local minima corresponding to ambiguities. Thus, with SeaWinds data, ambiguity selection is performed using a nudging/median filtering ambiguity selection step [7].

Although standard SeaWinds wind-only processing does not take into account rain effects, a probability-based rain flag known as the multidimensional histogram flag is used to indicate the presence of rain in SeaWinds data [15]. The MUDH flag is tuned to indicate rain if the probability of rain greater than 2 km · mm/h exceeds a threshold given a set of rain-sensitive parameters. The MUDH flag is compared to simultaneous wind/rain retrieval in Section IV.

III. Rain Estimate Accuracy

To evaluate the accuracy of SeaWinds-derived rain rates, we present mean and variance statistics obtained from the unbiased C–R bound and Monte Carlo simulations (see [7]). We demonstrate that the unbiased C–R bound matches simulation closely over much of the parameter space, but produces unreliable estimates in some situations due to biases in the estimation process. The standard deviation is shown to be generally less than half of the true rain rate value for most wind conditions.

A. Cramér–Rao Bound

The C–R bound gives a lower bound on the variance of an unbiased estimator [16] and has also been generalized to include biased estimators [17]. Let $\mathbf{p} = (u, d, R)^T$ be the estimation parameters for simultaneous wind/rain retrieval with u the wind speed in meters per second, d the wind direction in degrees, and R the rain rate in kilometers millimeters per hour. Also, let $\hat{\mathbf{p}}$ be the MLE estimate of the parameters. Using the notation of [12], the covariance $C(\mathbf{p})$ of a biased estimate given the measurements $\mathbf{z}$ is approximated by [18]

$$\begin{aligned}\boldsymbol{C}(\mathbf{p}) &= E\{[\hat{\mathbf{p}} - E\hat{\mathbf{p}}][\hat{\mathbf{p}} - E\hat{\mathbf{p}}]^T\} \\ &\gtrsim \frac{\partial E\hat{\mathbf{p}}}{\partial \hat{\mathbf{p}}} \boldsymbol{J}^{-1}(\mathbf{p}) \frac{\partial E\hat{\mathbf{p}}}{\partial \hat{\mathbf{p}}}^T \end{aligned} \tag{15}$$

where $E\{\cdot\}$ is the expectation operator and $\boldsymbol{J}(\mathbf{p})$ is the Fisher-information matrix given by

$$\boldsymbol{J}(\mathbf{p}) = E\left\{ \left[\frac{\partial L(\mathbf{p},\mathbf{z})}{\partial \mathbf{p}}\right]^T \frac{\partial L(\mathbf{p},\mathbf{z})}{\partial \mathbf{p}} \right\} \tag{16}$$

where $L(\mathbf{p},\mathbf{z})$ is the log-likelihood function of the maximum-likelihood probability equation.

If the estimator is unbiased (or biased by a constant value), the derivative of the estimate given in (15) reduces to the identity, and we have

$$\boldsymbol{C}(\mathbf{p}) \geq \boldsymbol{J}^{-1}(\mathbf{p}). \tag{17}$$

The solution of the Fisher-information matrix for the unbiased estimate corresponding to the scatterometer likelihood function of (13) is given in [12] and is equal to

$$J_{ij} = \sum_k \left[\frac{\partial \mathcal{M}_{rk}}{\partial p_i} \frac{1}{\varsigma_k^2} \frac{\partial \mathcal{M}_{rk}}{\partial p_j} + \frac{\partial \varsigma_{rk}^2}{\partial p_i} \frac{1}{2\varsigma_k^4} \frac{\partial \varsigma_{rk}^2}{\partial p_j} \right] \tag{18}$$

for the $\{i, j\}$th element of the matrix. Model function derivatives are numerically computed. Derivations of the rain model and variance gradients are given in [19].

Since the simultaneous wind/rain retrieval likelihood function has several maxima, each corresponding to a possible wind vector estimate, ambiguity selection must be taken into account in order to discuss statistics. In simulation, ambiguity selection is performed by selecting the ambiguity closest to the true wind in a vector sense. With the C–R bound, we cannot explicitly perform ambiguity selection. However, because the C–R bound is computed from derivatives evaluated at the true wind and rain, the computed variance is directly associated with the shape of the likelihood function surrounding the true wind and rain and not around the other ambiguities. Thus, the C–R bound inherently computes the variability of the ambiguity closest to the true wind. We can, thus, ignore ambiguity selection in the C–R bound analysis.

B. Cramér–Rao/Monte Carlo Simulation Analysis

As [7] suggests, the wind/rain MLE is somewhat biased. Thus, the most accurate representation of the MLE variance is the biased C–R bound [17]. However, the biased C–R bound requires knowledge of the derivative of the biased estimate, which is difficult to accurately compute. An approach to computing the bias derivative is given in [12].

Rather than compute the biased C–R bound, we compute the unbiased bound, which we compare to simulation results. Compass Monte Carlo simulations are performed in which wind and rain are simultaneously retrieved for a variety of wind/rain conditions and cross-track positions [7]. The simulation statistics are computed over 500 noise realizations for each set of conditions. Likewise, the unbiased C–R bound is computed. Standard deviation as a function of wind direction (relative to the direction of the satellite) and cross-track position are plotted in Figs. 1 and 2 for a wind speed of 7 m/s. For most sets of conditions in these examples, the C–R bound matches well with simulation results. We note that in some cases the simulation results are somewhat lower than the C–R bound because of biases in simultaneous wind/rain retrieval, and the fact that the model function derivatives are numerically obtained. In addition, there are extreme artifacts in the C–R bound at 60°, 120°, 240°, and 300°, and at nadir (evidenced by large error bounds, especially in the directional standard deviation). These artifacts are due significant biases in such regions. We recognize that these C–R bounds are not useful in such areas.

We note that the SeaWinds geometry was originally designed for wind observation and, thus, may be suboptimal for rain measurement. Nevertheless, the C–R bound and simulations suggest that rain can be retrieved to reasonable accuracy in most conditions. In Fig. 1, the standard deviation of the rain rate is generally less than half the true rain rate (excluding the swath edges). The rain rate standard deviation like that of the wind is dependent on cross-track position and peaks around nadir for all rain rates. This phenomenon is expected, as SeaWinds has degraded performance in the nadir region. The highest errors occur on the swath edges where insufficient azimuth looks render simultaneous wind and rain estimation unusable.

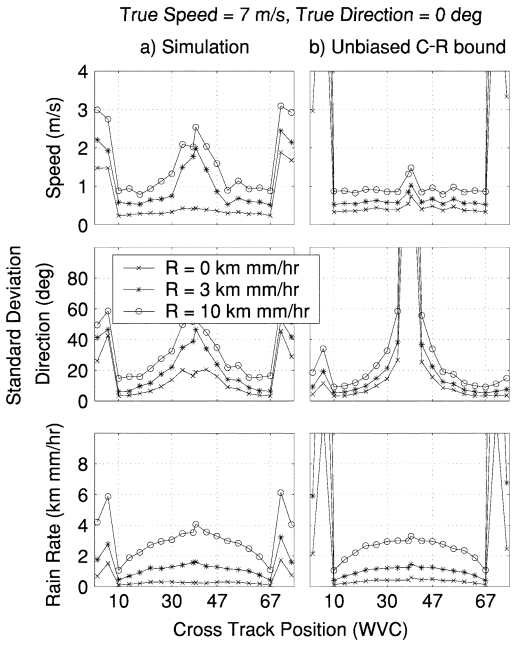

Fig. 1. Standard deviation as a function of cross-track position of retrieved wind speed, wind direction, and rain rate from QuikSCAT predicted via (a) simulation and (b) the unbiased C–R bound for three rain rates. Notice the anomalously large error in the nadir region for C–R directional standard deviation due to a bias in the estimate. The true wind velocity is 7 m/s and 0°.

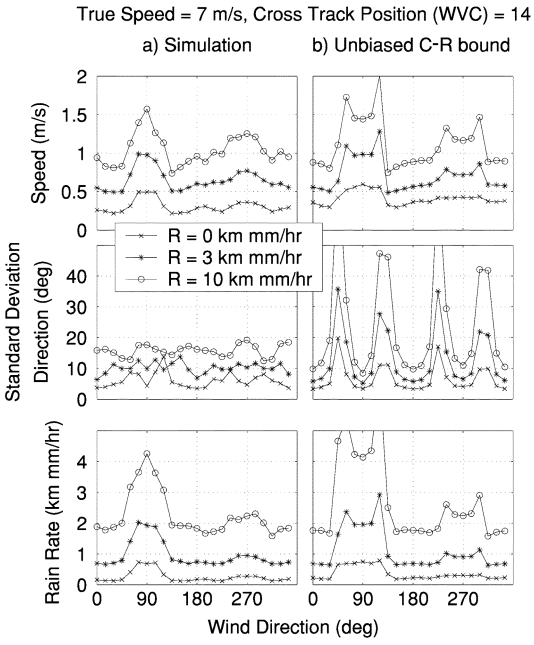

Fig. 2. Standard deviation as a function of wind direction of retrieved wind speed, wind direction, and rain rate from QuikSCAT predicted via (a) simulation and (b) the unbiased C–R bound for three rain rates. Notice the anomalous spikes at 60°, 120°, 240°, and 300° for the C–R bound, resulting from a bias in the estimate. The true wind speed is 7 m/s at cross-track position 14.

The rain rate standard deviations shown in Fig. 2 are reasonable for most wind directions, though noticeable peaks in the standard deviation occur at 90° and 270° relative to the motion of the satellite. These wind directions represent cross-swath blowing winds, where the wind backscatter response from the fore and aft beams equalize, similar to rain. Since these data

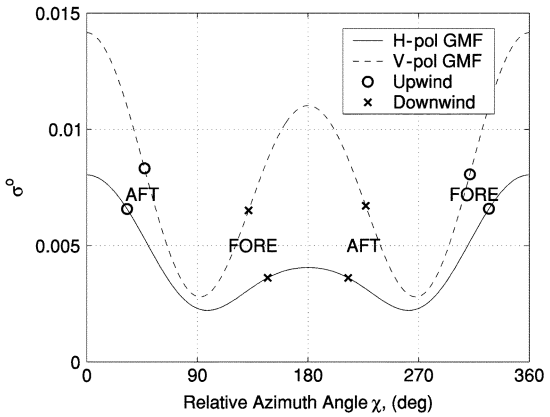

Fig. 3. GMF for a true wind speed of 7 m/s plotted for the inner H-polarization SeaWinds beam and outer V-polarization SeaWinds beam at WVC 14. Also plotted are the expected fore and aft backscatter measurements for each beam given an upwind direction (wind blowing toward the instrument or $d = 90°$ relative to the direction of the spacecraft motion), or a downwind direction (wind blowing away from the instrument or $d = 270°$ relative to the direction of the spacecraft motion).

are located in the left swath, a wind direction of 90° indicates wind blowing toward the satellite (upwind), while 270° is wind blowing away (downwind). For upwind measurements, the fore and aft azimuth angles are centered around a relative (to the wind) azimuth angle of $\chi = 0°$, while the downwind measurements are centered around a relative azimuth angle of $\chi = 180°$ (see Fig. 3). In Fig. 2, the standard deviation for the upwind measurements is somewhat higher than the standard deviation for downwind measurements. This phenomenon is related to the anisotropic nature of the GMF, illustrated in Fig. 3. For downwind measurements (measurements centered around a relative azimuth of $\chi = 0°$), the GMF reaches the global maximum for a given wind speed, while for downwind measurements (centered around $\chi = 180°$), a lower local maximum in the GMF occurs. Thus, for upwind measurements, the estimation procedure has a higher wind backscatter that it can mistakenly attribute to rain, creating larger errors in the rain measurement.

Besides a higher variance, another result of the wind/rain identifiability problem can be a bias in rain rate for certain conditions. The wind speed and rain rate bias is illustrated in Fig. 4 as a function of wind direction for various rain rates. The bias is dependent on rain rate, wind speed, wind direction, and cross-track position. The bias at zero-rain rate is partly due to the fact that the retrieved rain rate must be strictly nonnegative. The MLE estimates are biased positive near 90° and 270° where the backscatter signatures of wind and rain are most similar. As the rain rate increases, the variability of the estimate increases.

IV. Rain Rate Thresholding

The analysis from the C–R Bound and simulated data in Section III predict a bias and higher variability in the retrieved wind and rain for cross-swath winds. In addition, spurious rain rates may be generated by the estimation procedure. The spurious rain rates can be explained in the following way: As shown in Fig. 3, the V-polarization backscatter response for wind-roughened seas is higher than the H-polarization response. However, for rain backscatter, the opposite is true [5],

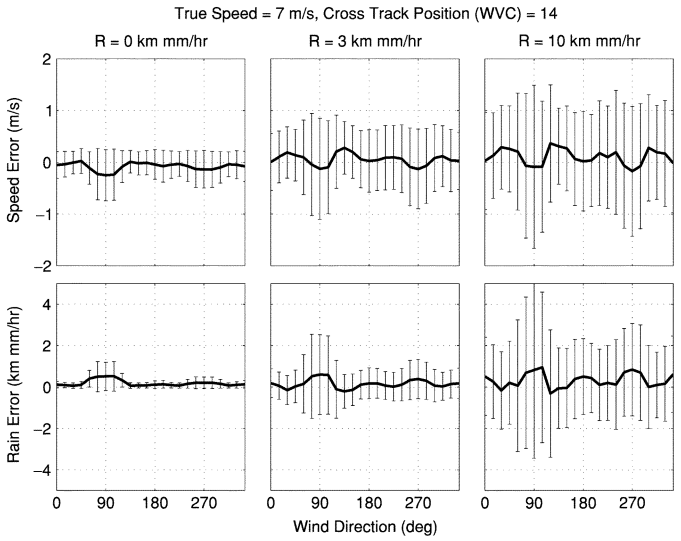

Fig. 4. (Line) Wind speed and rain bias and (error bars) standard deviations as a function of direction for several rain rates and a wind speed of 7 m/s for WVC 14, computed from simulation.

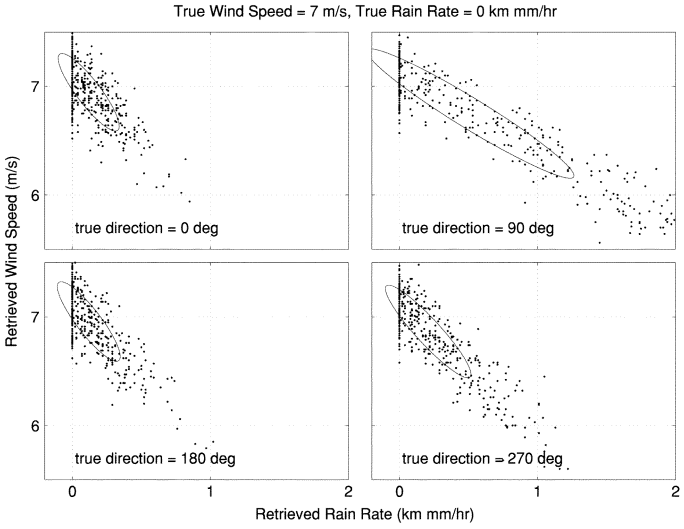

Fig. 5. Monte Carlo simulations of SeaWinds data at WVC 14 for several wind directions, a true wind speed of 7 m/s, and a true rain rate of 0 km · mm/h. Also shown are concentration ellipses representing the unbiased C–R bound.

[6], i.e., the H-polarization response is higher than V-polarization. Since noise perturbs the backscatter from the ideal GMF value, the observed V-polarization/H-polarization copolarization ratio is often smaller than expected (approximately half of the time). When the copolarization ratio is lower than average due to noise, and winds are pointing cross swath (resulting in an apparent "isotropic" backscatter between fore and aft beams), simultaneous wind/rain retrieval compensates by "adding rain" to the estimate in order to adjust for the lower copolarization ratio, and thus yielding a better fit to the data. The end result can be a spurious rain rate estimate. This phenomenon is illustrated in Fig. 5 for WVC 14, at a true rain rate of 0 km · mm/h. Because the true rain rate is 0 km · mm/h, the data points with nonzero rain represent spurious rain estimates. We note that spurious rain rates are most common for cross-swath-oriented winds.

Because spurious rain rates occur due to noise in the measurement, we assess the question of how well the retrieved rain represents a true rain event. From Fig. 5, most of the spurious rain rates are low. We can thus define a wind-dependent threshold below which QuikSCAT rain estimates should be ignored. Here, we calculate the threshold above which the estimation procedure produces few spurious rain rates. We examine two types of thresholds to ameliorate spurious rain rates: a constant rain rate threshold and a constant false-alarm threshold. Employing a constant rain rate threshold eliminates the low-end spurious rain rates (we note that most spurious rain rates have low magnitudes), and is simple to implement, but has varying performance depending on the vector wind and cross-track position. A constant false-alarm threshold applies a different threshold for each wind direction, speed, and cross-track position, but yields a constant false-alarm performance for all conditions, at the risk of missed detections. A combined approach is also addressed, which further reduces false alarms.

To generate the constant false-alarm thresholds, we choose the rain rate for which the simultaneous wind/rain retrieval estimates rain 1.5% of the time given zero-rain conditions. This is equivalent to setting a constant false-alarm rate of 1.5% for all wind/cross-track conditions. The threshold is computed for a wide range of cross-track positions, wind speeds, and wind directions. In doing so, we use the simulated data previously discussed. Thresholding the simultaneously retrieved rain rates gives a quality check of the rain data, and may be used as a rain flag; however, higher thresholds in some regimes cause a large number of missed rain detections.

The rain rate thresholds for various wind speeds, wind directions and cross-track positions are given in Fig. 6. The low threshold values for $u = 7$ m/s and $u = 11$ m/s illustrate that the simultaneous wind and rain retrieval does not significantly confuse rain and wind for low to moderate wind speeds. For higher winds, the rain flag thresholds are set high in the cross-swath directions because high spurious rain rates may occur there. These results suggest that in areas with low a average wind speed, such as the tropics, the simultaneous wind/rain procedure produces lower spurious rain rates. Therefore, the QuikSCAT-derived rain rates are of higher quality in the tropics than in higher wind speed regions, such as the mid- to high latitudes.

To validate the rain rate thresholds, we use three months of colocated TRMM PR data (see [6] for information on the colocation procedure). Ideally, rain rate thresholding uses the "true" wind velocity. Since using the retrieved wind speeds and directions is problematic during rain events, winds from the National Centers for Environmental Prediction (NCEP), available in the QuikSCAT Level 2B data, are used to index the thresholds. Before use, these wind estimates are adjusted for the bias due to differing reference heights [6]. The use of NCEP winds to index the thresholds introduces some variability into the rain flagging process, since NCEP winds at times may not accurately represent the true wind. However, in most conditions, especially when there are no fine-scale wind features, NCEP winds are adequate.

Table I shows the percentages of rain detections using no rain thresholding (any positive retrieved rain rate represent a rain detection), two constant rain thresholds (0.5 and 2.0 km

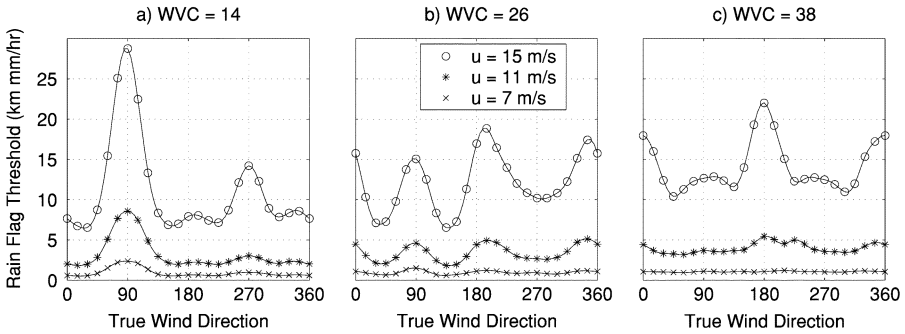

Fig. 6. Rain rate thresholds that yield a constant false-alarm rate of 1.5% given wind speed, wind direction, and cross-track position. The thresholds show the estimated rain rate below which SeaWinds rain estimates may not be valid given the wind conditions.

TABLE I
PERCENTAGE OF RAIN DETECTION FOR QUIKSCAT WITH NO-RAIN THRESHOLDING (N), WITH A CONSTANT 0.5-km · mm/h THRESHOLD (C0.5), WITH A CONSTANT 2.0-km · mm/h THRESHOLD (C2.0), WITH THE 1.5% FALSE-ALARM THRESHOLDS (F), WITH THE FALSE-ALARM THRESHOLDS COMBINED WITH A 0.5-km · mm/h LOWER LIMIT (CT). THE DATA ARE GIVEN FOR VARIOUS PR RAIN RATE (R_{PR}, KILOMETEERS PER MILLIMETER PER HOUR) BINS OVER THE COLOCATED TRMM/QUIKSCAT DATASET. ALSO SHOWN FOR COMPARISON ARE THE PERCENTAGES FLAGGED BY THE MULTIDIMENSIONAL HISTOGRAM FLAG [15]

R_{PR} bin	0 to 0.1	0.1 to 0.5	0.5 to 2	2 to 5	5 to 10	10 ↑
tot. num.	16007	3226	2266	1137	523	433
N	38.2%	59.2%	80.0%	90.9%	96.0%	98.2%
C0.5	10.0%	25.8%	63.6%	86.5%	94.4%	97.9%
C2.0	1.4 %	3.5%	16.6%	63.4%	91.6%	96.8%
F	2.9%	14.5%	43.6%	72.2%	88.5%	95.4%
CT	2.1%	10.6%	41.8%	71.9%	88.5%	95.4%
MUDH	2.1%	9.2%	31.7%	70.9%	95.0%	99.5%

· mm/h), and the 1.5% false-alarm thresholds for different ranges of PR-derived effective average rain rates (see [7]). Table I also shows a combined constant rain-rate/constant false-alarm threshold obtained by choosing the greater of the 1.5% false-alarm threshold and the 0.5-km · mm/h rain rate threshold. For comparison, the percentage of WVCs flagged by MUDH is displayed.

The first column of Table I displays the false-alarm rate (the percentage of cells with little or no rain that are flagged by the thresholding scheme). The following columns display the detection rates given various ranges of PR rain rates. Examining the "no-threshold" case (N), a large number of spurious rain rates are intrinsically generated by the estimation process. The 0.5-km · mm/h threshold reduces the false-alarm rate by a factor of 4. The threshold of 2.0 km · mm/h again reduces the false-alarm rate to a very reasonable amount, at the cost of missed detections.

The false-alarm rate for the constant false-alarm threshold is higher than expected (2.4%), suggesting the actual SeaWinds data may produce more spurious rain rates than simulated data. The combined threshold (CT) yields a very reasonable false-alarm rate of 2.1%, with very similar performance as MUDH. MUDH is slightly more effective at flagging the high-end rain, while CT is more sensitive at the lower rain rates. These results suggest that the simple thresholding scheme presented here produces better results than current rain flagging techniques at rain rates less than 5 km · mm/h. Future work is intended for more accurately flagging rain in SeaWinds data using both wind and rain rate estimates.

V. MONTHLY RAIN RATE VALIDATION WITH TMI

Validation studies with the TRMM Precipitation Radar [7] demonstrate that SeaWinds-derived rain estimates correlate quite well to active rain sensors, albeit SeaWinds operates on a much lower resolution. Here, we compare the SeaWinds rain data to a passive rain sensor by comparison of monthly rainfall averages between the TMI and QuikSCAT. In performing the comparison, simultaneous wind/rain retrieval is performed for four months of QuikSCAT data from August–November 1999. To help eliminate spurious rain rates, retrieved rain rates falling beneath the combined thresholds (CTs) are set to zero. The QuikSCAT retrieved rain rates and TMI surface rain rates are then gridded and averaged separately on a $1^\circ \times 1^\circ$ latitude–longitude grid.

The TMI surface rain rates give an estimate of the rain rate in millimeters per hour, customarily used for monthly observations. To convert to similar units as QuikSCAT, the TMI surface rain rate is multiplied by a monthly-average storm height (obtained from the $5^\circ \times 5^\circ$ PR 3A25 monthly-average data product, and interpolated to the $1^\circ \times 1^\circ$ grid) to yield an effective integrated average rain rate with units of kilometers millimeters per hour. We note that although we are examining integrated rain rate averages, SeaWinds rain data can be converted to the more customary units of millimeters per hour by dividing by the monthly storm height estimate. This may be more desirable for data fusion with PR or TMI.

An example comparison of the QuikSCAT/TMI monthly-average rain rates for August 1999 is given in Figs. 7 and 8. In this example, several global rain features are evident in both the TMI and QuikSCAT rain data. The major noticeable feature is the increased rain activity in the Inter-Tropical Convergence Zone (ITCZ) that stretches across the equator. Also, there is a noticeable correlation in the Southern Pacific Convergence Zone (SPCZ) located between -40° and -20° latitude and 150° and 270° longitude.

Table II gives the mean bias, error standard deviation, and rms error statistics (QuikSCAT-TMI) along with correlation coefficients for four months of data. Data points falling greater than five standard deviations from the mean are discarded. Overall, the QuikSCAT data is biased slightly low for all months. The bias is about 20% of the mean TMI rain rate. This bias is comparable to the bias first reported in monthly comparisons between the Special Sensor Microwave/Imager and TMI [20]. The bias is expected due to the fact that some true rain events are ignored

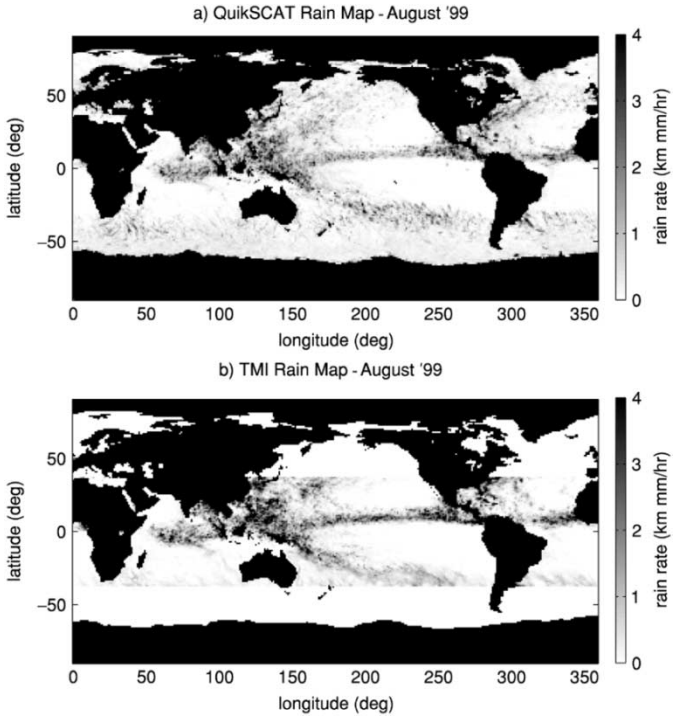

Fig. 7. Monthly rain rate average for (a) QuikSCAT-derived rain rates using the combined rain threshold and (b) TMI-derived rain rates.

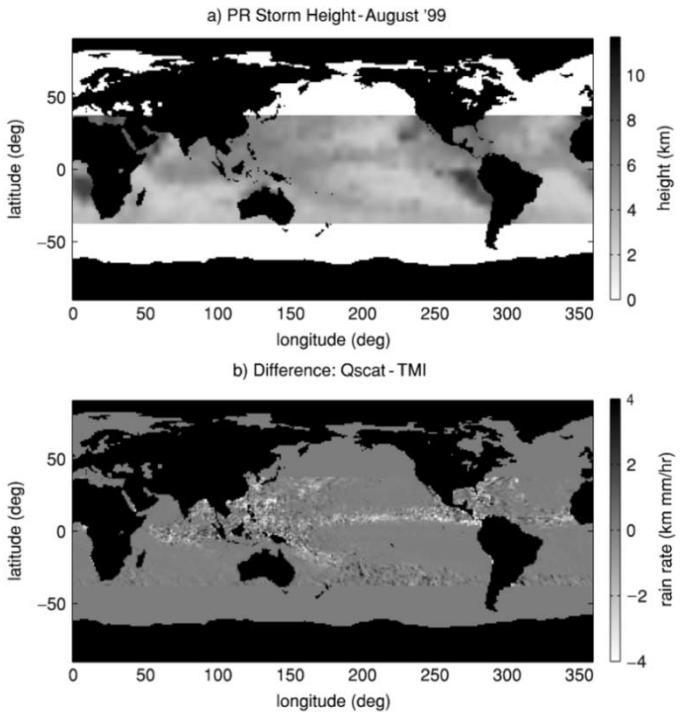

Fig. 8. (a) Monthly rain height average from TRMM PR, interpolated to $1^\circ \times 1^\circ$ grid. (b) Error between QuikSCAT and TMI monthly-average rain rate for August 1999.

by the rain thresholding. Overall, the correlation coefficients for the QuikSCAT and TMI data are around 0.7 for the monthly averages. A histogram of QuikSCAT versus TMI monthly data for August 1999 is given in Fig. 9, illustrating the variability of the QuikSCAT versus the TMI measurements. The overall standard deviation of the difference is about 0.7 km · mm/h.

TABLE II
MEAN BIAS (KILOMETERS PER MILLIMETER PER HOUR), ERROR STANDARD DEVIATION, RMS ERROR, AND CORRELATION COEFFICIENTS FOR MONTHLY AVERAGES OF QUIKSCAT-DERIVED RAIN RATES AND TMI RAIN RATES. A POSITIVE MEAN BIAS INDICATES LARGER AVERAGE QUIKSCAT RAIN RATES. A NEGATIVE BIAS INDICATES LARGER TMI RAIN RATES

	08-99	09-99	10-99	11-99
mean bias (km mm/hr)	-0.09	-0.10	-0.14	-0.13
error std (km mm/hr)	0.69	0.70	0.68	0.70
rms error (km mm/hr)	0.69	0.70	0.69	0.71
corr. coef.	0.75	0.74	0.75	0.68

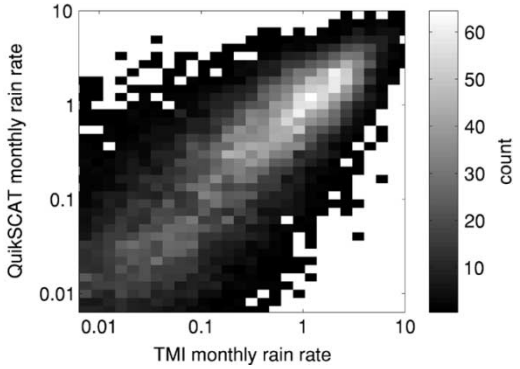

Fig. 9. Comparison histogram of monthly averages between QuikSCAT and TMI.

A noticeable difference between the TMI and QuikSCAT monthly rain maps is the noisy nature of the QuikSCAT rain rates in the SPCZ, whereas the TMI data is much smoother. Part of the difference is due to the fact that the TMI data has much higher coverage of this area. For the one month dataset, the TMI data has over 2000 data points per pixel in the southern tropics, while the QuikSCAT data has less than 1000 data points per pixel. Thus, the higher coverage allows for a more consistent time average of the region.

The difference map shows occasional high discrepancies between QuikSCAT and TMI rain rates. Part of the variability is due to the fact that measurements were taken at different times for the QuikSCAT and TMI datasets. In addition, poor temporal sampling for the two instruments introduces errors in both datasets. Histograms of the rain rate provide a useful comparison tool for the datasets. Fig. 10 shows a histogram of the monthly-averaged rain rates for both TMI and QuikSCAT. The histograms match very well at low rain rates, but show a small negative bias for QuikSCAT data at higher rain rates. Because the shape of the curves are very similar, it is likely that the rain rate bias can be eliminated by adjusting the QuikSCAT values, effectively moving the QuikSCAT curve to the right and better matching the TMI curve.

We extend the QuikSCAT-TMI comparison by computing the monthly-averaged statistics for August 1999 for four different areas in the Pacific Ocean: -40° to -20° (SPCZ), -20° to 0° (Dry Southern Pacific Zone, S. Dry), 0° to 20° (ITCZ), 20° to 40° (Dry Northern Pacific Zone, N. Dry) in Table III. The dry zones have lower errors and higher correlation coefficients, owing to the fact that the rain rates are lower in these regions. The largest bias is noticed in the ITCZ, where the QuikSCAT data is on average about 0.3 km · mm/h lower than the TMI data. In the SPCZ, the noisy rain estimates result in a lower

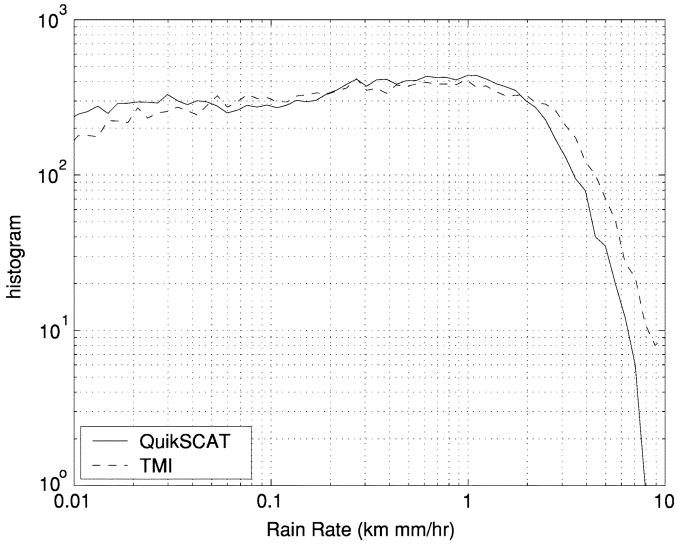

Fig. 10. Histogram of monthly-averaged rain rate values obtained from QuikSCAT and TMI for August 1999.

TABLE III
ERROR STATISTICS OF THE AVERAGE QUIKSCAT-DERIVED RAIN RATES AND TMI RAIN RATES PER LATITUDE BAND IN THE PACIFIC OCEAN FOR THE MONTH OF AUGUST, 1999

	-40° to -20° SPCZ	-20° to 0° S. DRY	0° to 20° ITCZ	20 to 40° N. DRY
mean bias*	0.07	-0.07	-0.30	-0.08
error std*	0.54	0.42	0.81	0.48
rms error*	0.55	0.43	0.86	0.49
corr. coef.	0.45	0.81	0.71	0.71

*km mm/hr

correlation coefficient for the region than in other areas. The bias, however, is much smaller in the SPCZ than the bias in other areas of heavy rainfall.

Although somewhat biased, QuikSCAT rain measurements can be adjusted in the mean to give an unbiased comparison with TMI. Rain measurement with QuikSCAT can complement other active sensors such as the PR, since it has a much wider swath, and obtains coverage over the poles, albeit at lower resolution.

VI. CONCLUSION

Although designed to measure near-surface winds, the SeaWinds instrument is also sensitive to rain and thus can be used for global rain measurement. Using the simultaneous wind/rain retrieval method described in [7], rain rate estimates consistent with passive and active instruments such as the PR and TMI can be obtained.

This paper addresses the quality and validity of SeaWinds rain measurements. For wind not pointing cross swath, the rain retrieval standard deviation is generally within 3 dB of the true rain, with increased performance in the sweet spots. In cross-swath wind orientations, spurious rain rates often occur and the retrieved rain rate is biased somewhat high. The problem is evidenced in the Cramér–Rao lower bound and in Monte Carlo simulations. Because the wind and rain signals may not be completely separable in such orientations, a rain thresholding scheme is developed which is set higher in regions of poor wind/rain identifiability to reduce the false alarms. These thresholds are validated with TRMM PR and shown to yield similar rain flagging results as the MUDH flag. Further improvement of the rain flag is forthcoming.

The rain rate thresholds illustrate that for moderate wind speeds (3–10 m/s), the retrieved rain rates are valid as low as 0.5 km · mm/h for most wind directions. For wind speeds less than 11 m/s, the rain rates are valid as low as 2 km · mm/h, except for cross-swath-oriented winds. For higher wind speeds, however, there exists a nonnegligible rain rate regime for which the validity of the retrieved rain rate is questionable.

Validation of QuikSCAT rain rates with TMI illustrates the utility of using Ku-band scatterometer data from instruments such as SeaWinds to measure rain. In addition, SeaWinds affords further active rain measurement to supplement the data obtained by other active instruments such as the PR. Using the simultaneous wind/rain retrieval technique and rain rate thresholding, the QuikSCAT-derived rain rates are shown to be consistent with monthly averages derived from TMI. We note that the method analyzed in this paper estimates the vertically integrated rain rate in kilometers millimeters per hour and thus requires storm height estimates or a storm model to yield the more common rain measurement in millimeters per hour (customarily used for monthly rain observation). Once a storm height estimate is applied, the QuikSCAT-derived rain rates can be used for supplemental monthly observation of accumulated rainfall.

REFERENCES

[1] F. T. Ulaby, R. K. Moore, and A. K. Fung, *Microwave Remote Sensing Active and Passive*. Norwood, MA: Artech House, 1981.
[2] L. F. Bliven and J. P. Giovanangeli, "Experimental study of microwave scattering from rain- and wind-roughened seas," *Int. J. Remote Sens.*, vol. 14, pp. 855–869, 1993.
[3] R. F. Contreras, W. J. Pland, W. C. Keller, K. Hayes, and J. Nystuen, "Effects of rain on Ku-band backscatter from the ocean," *J. Geophys. Res.*, vol. 108, no. C5, pp. (34)1–(34)15, 2003.
[4] D. E. Weissman, M. A. Bourassa, and J. Tongue, "Effects of rain rate and wind magnitude on SeaWinds scatterometer wind speed errors," *J. Atmos. Ocean. Tech.*, vol. 19, no. 5, pp. 738–746, May 2002.
[5] B. W. Stiles and S. Yueh, "Impact of rain on spaceborne Ku-band wind scatterometer data," *IEEE Trans. Geosci. Remote Sensing*, vol. 40, pp. 1973–1983, Sept. 2002.
[6] D. W. Draper and D. G. Long, "Evaluating the effect of rain on SeaWinds scatterometer measurements," *J. Geophys. Res.*, vol. C12, 2004. DOI: 10.1029/2002JC001741.
[7] ——, "Simultaneous wind and rain retrieval using SeaWinds data," *IEEE Trans. Geosci. Remote Sensing*, vol. 42, pp. 1411–1423, July 2004.
[8] C. Kummerow, J. Simpson, O. Thiele, W. Barnes, A. T. C. Chang, E. Stocker, R. F. Adler, A. Hou, R. Kakar, F. Wentz, P. Ashcroft, T. Kozu, Y. Hong, K. Okamoto, T. Iguchi, H. Kuroiwa, E. Im, Z. Haddad, G. Huffman, B. Ferrier, W. W. Olson, E. Zipser, E. A. Smith, T. T. Wilheit, G. North, T. Krishnamurti, and K. Nakamura, "The status of the Tropical Rainfall Measuring Mission (TRMM) after two years in orbit," *J. Appl. Meteorol.*, vol. 39, pp. 1965–1982, Dec. 2000.
[9] M. W. Spencer, C. Wu, and D. G. Long, "Tradeoffs in the design of a spaceborne scanning pencil beam scatterometer: Application to SeaWinds," *IEEE Trans. Geosci. Remote Sensing*, vol. 35, pp. 115–126, Jan. 1997.
[10] S. J. Shaffer, R. S. Dunbar, S. V. Hsiao, and D. G. Long, "A median-filter-based ambiguity removal algorithm for NSCAT," *IEEE Trans. Geosci. Remote Sensing*, vol. 29, pp. 167–174, Jan. 1991.
[11] B. W. Stiles, B. D. Pollard, and R. S. Dunbar, "Direction interval retrieval with thresholded nudging: A method for improving the accuracy of QuikSCAT winds," *IEEE Trans. Geosci. Remote Sensing*, vol. 40, pp. 79–89, Jan. 2002.
[12] T. E. Oliphant and D. G. Long, "Accuracy of scatterometer derived winds using the Cramér–Rao bound," *IEEE Trans. Geosci. Remote Sensing*, vol. 37, pp. 2642–2652, Nov. 1999.

[13] D. G. Long and M. W. Spencer, "Radar backscatter measurement accuracy for a spaceborne pencil-beam wind scatterometer with transmit modulation," *IEEE Trans. Geosci. Remote Sensing*, vol. 35, pp. 102–114, Jan. 1997.
[14] C. Chi and F. K. Li, "A comparative study of several wind estimation algorithms for spaceborne scatterometers," *IEEE Trans. Geosci. Remote Sensing*, vol. 26, pp. 115–121, Mar. 1988.
[15] J. N. Huddleston and B. W. Stiles, "A multi-dimensional histogram rain flagging technique for SeaWinds on QuikSCAT," in *Proc. IGARSS*, vol. 3, Honolulu, HI, 2000, pp. 1232–1234.
[16] T. K. Moon and W. C. Stirling, *Mathematical Methods and Algorithms for Signal Processing*. Upper Saddle River, NJ: Prentice-Hall, 2000.
[17] J. A. Fessler, "Mean and variance of implicitly defined biased estimators (such as penalized maximum likelihood): Applications to tomography," *IEEE Trans. Image Processing*, vol. 5, pp. 493–506, Mar. 1996.
[18] L. L. Scharf, *Detection, Estimation and Time Series Analysis*. Reading, MA: Addison-Wesley, 1999.
[19] D. W. Draper, "Wind scatterometry with improved ambiguity selection and rain modeling," Ph.D. dissertation, Brigham Young Univ., Provo, UT, 2003.
[20] A. T. C. Chang, L. S. Chiu, J. Meng, and T. Wilheit, "First results of the TRMM Microwave Imager (TMI) monthly oceanic rain rate: Comparison with SSM/I," *Geophys. Res. Lett.*, vol. 26, pp. 2379–2382, 1999.

David W. Draper received the Ph.D. degree in electrical engineering from Brigham Young University (BYU), Provo, UT, in 2003. His Ph.D. research included remote sensing of ocean winds and rain using satellite scatterometer data.

He is currently a Systems Engineer with Ball Aerospace, Boulder, CO. In 1999, he joined the Microwave Earth Remote Sensing research group, BYU. He has developed algorithms to identify typical errors in scatterometer wind estimation and is using wind and rain models to improve the wind estimation technique.

Dr. Draper is a Tau Beta Pi Fellow (2000–2001).

David G. Long (S'80–SM'98) received the Ph.D. degree in electrical engineering from the University of Southern California, Los Angeles, in 1989.

From 1983 to 1990, he was with the National Aeronautics and Space Administration (NASA) Jet Propulsion Laboratory (JPL), Pasadena, CA, where he developed advanced radar remote sensing systems. While at JPL, he was the Senior Project Engineer on the NASA Scatterometer (NSCAT) project, which was flown aboard the Japanese Advanced Earth Observing System (ADEOS) from 1996 to 1997. He was also the Experiment Manager and Project Engineer for the SCANSCAT scatterometer (now known as SeaWinds). In 1990, he joined the Department of Electrical and Computer Engineering, Brigham Young University (BYU), Provo, UT, where he currently teaches upper division and graduate courses in communications, microwave remote sensing, radar, and signal processing, is the Director of BYU's Center for Remote Sensing, and is the Head of the Microwave Earth Remote Sensing Laboratory. He is the Principal Investigator on several NASA-sponsored interdisciplinary research projects in microwave remote sensing and innovative radar systems. He has numerous publications in signal processing and radar scatterometry. His research interests include microwave remote sensing, radar, polar ice, signal processing, estimation theory, and mesoscale atmospheric dynamics. He has over 250 publications in the open literature.

Dr. Long has received the NASA Certificate of Recognition several times.